Analytical Biochemistry 469 (2015) 19–26

Contents lists available at ScienceDirect

Analytical Biochemistry

journal homepage: www.elsevier.com/locate/yabio

Design of turbulent tangential micro-mixers that mix liquids on the nanosecond time scale

Sandra Mitic [a], Jan W. van Nieuwkasteele [b], Albert van den Berg [b], Simon de Vries [a,*]

[a] Laboratory of Biotechnology, Delft University of Technology, 2628 BC Delft, The Netherlands
[b] BIOS/Lab-on-a-Chip group, MESA+ Institute for Nanotechnology and MIRA Institute for Biomedical Technology, University of Twente, 7500 AE Enschede, The Netherlands

ARTICLE INFO

Article history:
Received 30 May 2014
Received in revised form 3 October 2014
Accepted 8 October 2014
Available online 16 October 2014

Keywords:
Ultrafast mixing
Kinetics
Biocatalysis

ABSTRACT

Unravelling (bio)chemical reaction mechanisms and macromolecular folding pathways on the (sub)microsecond time scale is limited by the time resolution of kinetic instruments for mixing reactants and observation of the progress of the reaction. To improve the mixing time resolution, turbulent four- and two-jet tangential micro-mixers were designed and characterized for their mixing and (unwanted) premixing performances employing acid–base reactions monitored by a pH-sensitive fluorescent dye. The mixing performances of the micro-mixers were determined after the mixing chamber in a free-flowing jet. The premixing behavior in the vortex chamber was assessed in an optically transparent glass–silicon replica of a previously well-characterized stainless-steel four-jet tangential micro-mixer. At the highest flow rates, complete mixing was achieved in 160 ns with only approximately 9% premixing of the reactants. The mixing time of 160 ns is at least 50 times shorter than estimated for other fast mixing devices. Key aspects to the design of ultrafast turbulent micro-mixers are discussed. The integration of these micro-mixers with an optical flow cell would enable the study of the very onset of chemical reactions in general and of enzyme catalytic reactions in particular.

Studies to delineate the mechanism of (bio)chemical reactions are performed in either of two different ways. A reaction can be initiated by rapidly mixing two or more reactants, or an initial equilibrium is suddenly disturbed, for example, by a short laser pulse, so-called relaxation techniques [1,2]. Thanks to the development of the laser during the 1960s and of ultrafast lasers during the past two decades, the time resolution of relaxation techniques is below femtoseconds, enabling characterization of ultra-transient states in chemical reactions or determination of the (sub)picosecond kinetics of electron transfer in photochemically activated reaction centers of chloroplasts and photosynthetic microorganisms [3,4]. The time resolutions for turbulent mixing and subsequent observation in stopped-flow (~0.5–1 ms [5,6]) and continuous-flow (~11–50 μs [7–9]) mixing instruments are much lower than those for relaxation techniques. The shortest time scale for protein and RNA folding or breaking and making chemical bonds in reactions catalyzed by enzymes is 0.1 to 1 μs [1,2,8–14] and, thus, is not accessible with mixing techniques. Fast enzymes with kinetic phases on the (sub)microsecond time scale include many members of the oxidoreductases (e.g., catalase, cytochrome oxidases), hydrolases (e.g., acetylcholinesterase), and lyases (e.g., carbonic anhydrase) but are also found within the isomerases and ligases. In general, the reaction progress of oxidoreductases can be monitored by ultraviolet–visible (UV–vis)[1] spectroscopy or vibrational spectroscopy because they often contain heme centers [2]; fluorescence spectroscopy is more appropriate for the study of the other classes of enzymes. To approach the time scale of 0.1 to 1 μs experimentally, the need for mixing reactants can be obviated by the application of cage compounds, that is, photolabile substrate analogues that are premixed with the enzyme and activated on a (laser) flash of light [1,2,15,16]. However, the study of the catalytic cycle of the great majority of enzymes requires that enzyme and substrate be rapidly mixed. A comparison of the shortest time scales of enzyme-catalyzed reactions and of the best mixing instruments indicates the need to improve the mixing time resolution of the kinetic equipment in particular to record as many transient states as possible to define the catalytic mechanism.

The first instrument with subsecond time resolution developed to mix two solutions was described in 1923 by Hartridge and Roughton. This continuous-flow instrument with its inherent high

* Corresponding author. Fax: +31 152782355.
E-mail address: s.devries@tudelft.nl (S. de Vries).

[1] *Abbreviations used:* UV–vis, ultraviolet–visible; HPLC, high-performance liquid chromatography; HPTS, 8-hydroxypyrene-1,3,6-trisulfonic acid.

http://dx.doi.org/10.1016/j.ab.2014.10.003
0003-2697/

sample consumption rate employed a four-jet tangential mixer (dead time of ~10 ms [17]; improved a few years later to ~2 ms [18]) and was used to study the binding kinetics of O_2 to hemoglobin by means of UV–vis spectroscopy. The long axis of the transparent flow tube served as the time axis; optical changes were monitored perpendicular to the long axis. The next development in time resolution (~1 ms) along with a great reduction in sample consumption was the stopped-flow instrument designed in 1940 by Chance [19]. The time resolution of this now widely used instrument cannot be significantly improved to below approximately 0.5 ms, in spite of miniaturization, because it is determined by the speed of arresting the fluid flow. The stopped-flow instrument allows detection of reactions by UV–vis and fluorescence spectroscopy, circular dichroism, Fourier transform infrared, resonance Raman spectroscopy, nuclear magnetic resonance, or X-ray absorption spectroscopy [2]. Significant improvements in mixing time resolution are achieved with the continuous-flow instruments designed in 1998 by Röder and coworkers [7,8,20,21] and in 2007 by Takahashi's group [9] that enable UV–vis and fluorescence detection. The instrument designed by Röder employs a capillary micro-mixer with smallest channel dimensions of approximately 200 μm where the flow is laminar and a Pt ball to mix the reactants in 10 to 15 μs by turbulent mixing. The total dead time for observation of this instrument amounts to approximately 50 μs, which includes the mixing time, the dead volume, and the time to fill the observation chamber. In the instrument designed by Takahashi, the reagent flows are nonlaminar before mixing, which increases the mixing efficiency when the flows collide, decreasing the dead time to approximately 11 μs. An important key to improve the mixing time resolution in these latter studies was miniaturization of the flow channels (~10 μm [9]), leading to smaller dead volumes and, hence, to shorter dead times.

Micro-mixers (channels ~ <500 μm) are mostly used in "lab-on-a-chip" devices for analytical purposes [22–24]. The use of microfabricated structures and microfluidics offers many advantages, including new functionalities, higher throughput, reduced sample consumption, shorter analysis time, and reduced operating and manufacturing costs [23,25,26]. However, the majority of the micro-mixers used in lab-on-a-chip devices usually operate in the laminar flow regime at low Reynolds numbers (<100) that generally limits their mixing efficiency and time resolution, in particular in the case of simple mixer geometries (T- and Y-mixers). The efficiency or degree of mixing depends on the dimensionless Reynolds number, *Re*. Rapid and complete mixing requires turbulent flow conditions to disperse the reactants to the molecular level of the solvent(s) so that the collision rate of the reactants is governed only by diffusion. The transition from laminar to turbulent flow occurs at *Re* ~2000 for flow in pipes [27], where *Re* is given by the equation

$$Re = \frac{\rho \times < \upsilon > \times d}{\eta}. \quad (1)$$

where ρ is the solvent density (equal to 1000 kg m^{-3} for water at 20 °C), $< \upsilon >$ is the linear average flow velocity of the liquid in a channel (m s^{-1}), d is the hydraulic diameter of the channel (m), and η is the dynamic viscosity (equal to 10^{-3} kg m^{-1} s^{-1} for water at 20 °C). To enter the turbulent regime in micro-channels of 100 μm, linear flow rates greater than 20 m s^{-1} are required. Such high flow rates lead to a buildup of pressure (ΔP) according to Bernoulli's velocity/dynamic pressure equation [28]:

$$\Delta P = 0.5 \cdot \rho \cdot (< \upsilon >)^2. \quad (2)$$

The calculated pressure for the turbulent regime in channels of 100 μm amounts to at least 0.2 MPa but may be as high as 0.5 to 1 MPa in practice due to wall friction and increased viscosity of concentrated solutions. Pressures greater than 0.2 MPa are much higher than those usually generated by the hydrodynamic flows in μTAS (micro total analysis system) and MEMS (micro electromechanical system) devices [29]. High pressures require a robust design that appears to be incompatible with the majority of lab-on-a-chip devices. For these reasons, many types of micro-mixers for lab-on-a-chip applications that operate at low hydrodynamic pressures [23,30] while able to mix reactants in approximately 1 ms have been designed. This is achieved by introducing complex premixing geometries that generally increase the contact areas between the reactant flows [28–35]. For example, contact areas can be increased by splitting incoming flows into several narrower streams that later join as described for 4-jet and 16-jet tangential mixers [28,32].

In hydrodynamic focusing devices, a thin stream of, for example, a protein solution is squeezed between two reagent streams [2,36–42]. The small width and depth dimensions of the stream carrying the protein solution (~30 nm–1 μm and ~10 μm, respectively) allow rapid diffusive mixing (~4–10 μs and with a claim of only ~1 μs [39]) with the reagent with minimal protein consumption [41,42]. Thus, protein and RNA folding intermediates that occur on a short time scale could be studied by fluorescence spectroscopy, in particular by FRET (Förster resonance energy transfer) [41,42].

Inspired by the developments listed above, we were interested in the design requirements for turbulent micro-mixers with mixing times in the (sub)microsecond time domain for use in real-time spectroscopic instruments for the characterization of ultra-transient intermediates. Premixing in such mixers should, in contrast to mixers used in lab-on-a-chip application, be minimized and preferably be absent because it significantly adds to the dead time for observation. In view of this, the authors previously designed a stainless-steel turbulent four-jet tangential micro-mixer with channels of 100 μm, enabling maximal linear flow rates of 200 m s^{-1} and maximal operating pressures of 40 MPa [28]. This mixer was integrated in an ultrafast freeze-quench instrument that achieves a shortest dead time of 75 μs [28,43,44]. In this stainless-steel micro-mixer, mixing appeared to be completed within approximately 2 μs [28], which is at least five times faster than in Refs. [7,8]. However, given a smallest mixing volume of 10 pl, the true mixing time of this stainless-steel mixer can be calculated as approximately 160 ns (cf. Fig. 1). Precise knowledge of the mixing time was not so important for the freeze-quench procedure because the time resolution of the setup is determined mainly by the 40- to 50-μs freezing time. However, exact knowledge of the premixing and mixing behavior, which determines the total mixing time, is a prerequisite to successful integration of this or like mixers in future ultrafast real-time optical applications [7,8]. To validate the calculated mixing time of 160 ns, we designed several four-jet and two-jet turbulent micro-mixers that are optically transparent analogues of the stainless-steel four-jet tangential micro-mixer and determined their premixing and mixing times. The results show that mixing liquids on the nanosecond time scale is possible, and guidelines to build instruments for kinetic research with the highest possible time resolution are discussed.

Materials and methods

We previously designed a stainless-steel four-jet tangential micro-mixer (Fig. 1) capable of completely mixing two liquids within 2 μs [25]. High flow rates that generate sufficient turbulence for complete mixing of (viscous) solutions were obtained with two high-performance liquid chromatography (HPLC) pumps with a 40-MPa pressure limit described previously [25,33,34]. In this work, we report the properties of replicas of this stainless-steel micro-mixer with minor variations. Mixers were made from

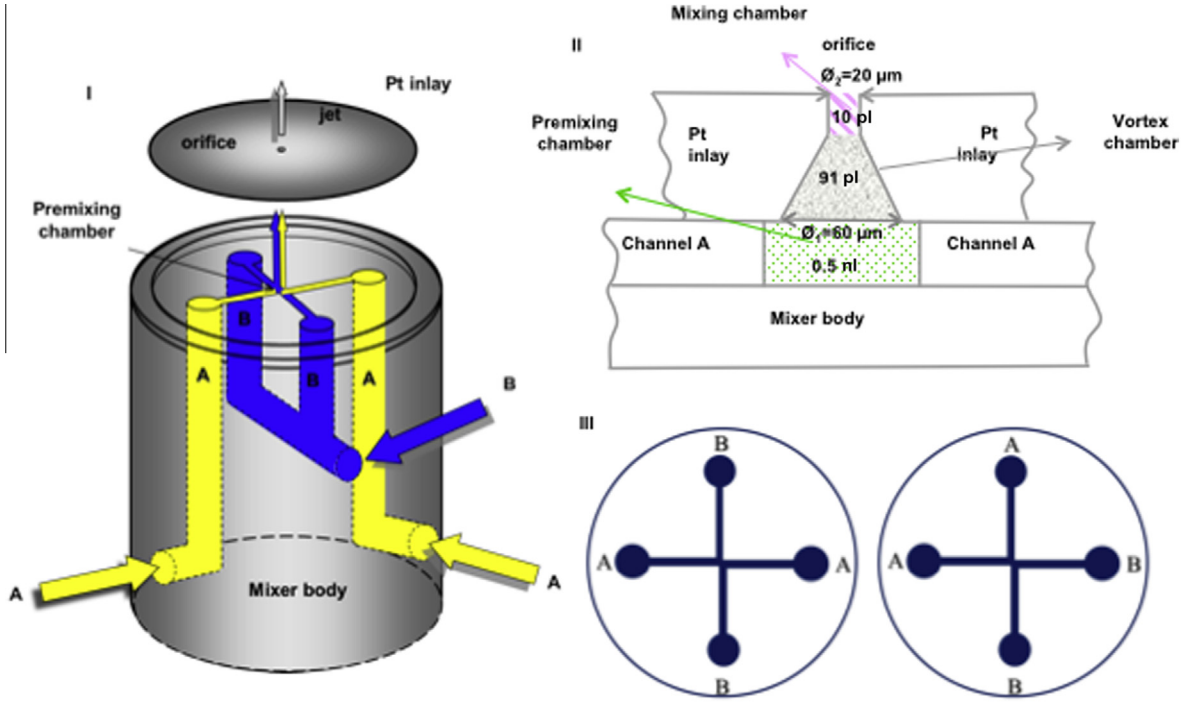

Fig.1. Schematic drawing of the four-jet tangential ABAB stainless-steel micro-mixer and its Plexiglass analogues. (I) The stainless-steel micro-mixer as designed in Ref. [25]. Reactants A and B enter the mixer body as shown, are subsequently split, and meet at a "cross," the premixing chamber. Liquids may meet in the ABAB (III) or AABB (IV) arrangement. (II) After the premixing chamber, the fluids enter the vortex chamber (shown as cross section; in the AABB mixer, channel A and channel B would meet) present in the *Pt* inlay and are then forced through the orifice. The *Pt* inlay is fitted to the mixer body by a brass screw cap (not shown; see in Ref. [6]). The channels are offset (III, IV), by a full-width (stainless-steel) or two-thirds width (Plexiglass) of the channel.

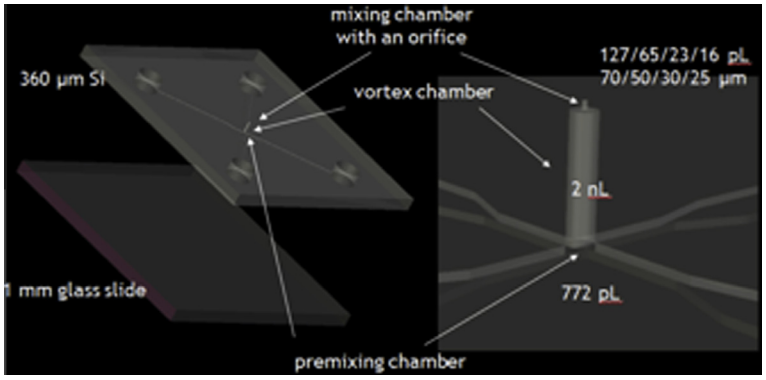

Fig.2. Design and geometry of the four-jet tangential ABAB glass–silicon micro-mixer chips with orifice diameters of 25, 30, 50, and 70 µm.

Plexiglass or from glass–silicon. The stainless-steel and Plexiglass micro-mixers were used to quantitatively determine the final mixing performance by measuring fluorescence appearance in a free-flowing jet. We also constructed an optically transparent glass–silicon chip with a four-jet tangential mixer to quantitatively determine the premixing profile. Each mixing setup consists of a mixer body connected to the HPLC solvent delivery system and, as defined below, comprises a premixing chamber, a vortex chamber, and a mixing chamber. The (mixed) reactants leave the mixing chamber, which is essentially an orifice, as a free jet (see Figs. 1 and 2). The glass–silicon mixer did not, however, produce a stable free-flowing jet, preventing direct quantitative determination of its final mixing performance. The high flow rates used in this work require high pressures. Approximately 30% of the glass–silicon mixers remained intact at pressures up to 10 to 15 MPa. The glass–silicon chip was fabricated using standard micro-fabrication techniques with one Pyrex glass wafer and one double-sided polished silicon wafer, standard substrate cleaning steps, (three) film photoresist deposition steps and (three) photolithography steps, and a glass–silicon anodic thermal bonding step, as outlined in Ref. [45]. The channel etching in the silicon was done by the dry etching Bosch process.

Micro-mixer designs

The schematics of the setup and dimensions of the mixers are shown in Figs. 1 and 2 and Table 1. The two reactants, A and B, are delivered from sample bottles by two HPLC pumps (Schimadzu LC-20AT and Waters 515) into the mixer body as in the MHQ (microsecond freeze-hyperquenching) setup [25]. Reactant channels are 300 µm in diameter for the four-jet tangential ABAB stainless-steel mixer and all of the Plexiglass mixers or 500 µm in diameter for the four-jet tangential ABAB glass–silicon micro-mixer chips (Fig. 2). These wide channels narrow to micro-channels

Table 1
Dimensions of micro-mixers.

	Type of mixer		
	Stainless steel[a]	Plexiglass[a]	Glass silicon
Solvent inlet channel (diameter, μm)	300	500	500
Premixing chamber inlet channel (depth, width, μm)	50, 50	60, 60	70, 70
Premixing chamber (length, width, depth, μm) (volume, nl)	100, 100, 50 $V = 0.50$	100, 100, 60 $V = 0.60$	105, 105, 70 $V = 0.77$
Vortex chamber (diameters $Ø_1$–$Ø_2$, length, μm) (volume, nl)	Conical 60–20 × 67 $V = 0.09$	Conical 60–20 × 67 $V = 0.09$	Cylindrical 100 × 257 $V = 2$
Mixing chamber (diameter, length, μm) (volume, pl)	Cylindrical 20 × 33 $V = 10$	Cylindrical 20 × 33 $V = 10$	Cylindrical 25/30/50/70 × 33 $V = 16, 23, 65, 127$

[a] The vortex chambers and mixing chambers of the stainless-steel and Plexiglass mixers are located in the *Pt* seal (Figs. 1 and 2).

within the mixer body and meet at a cross section, the "premixing chamber." The micro-channels (50, 60, or 70 μm wide and deep; see Table 1) are offset with respect to each other by a full-width of the channel in the four-jet tangential ABAB stainless-steel mixer, by two-thirds of the channel width in all of the Plexiglass mixers, or by a half-width of the channel in the four-jet tangential ABAB glass–silicon micro-mixer chips. For example, the dimensions of the premixing chamber (in width × width × depth) are 100 × 100 × 50 μm (0.50 nl volume) for the four-jet tangential ABAB stainless-steel mixer (Table 1). The offset of the channels induces a vortex in which the four (or two in the case of the two-jet tangential mixer) liquid streams rotate around one another. After the premixing chamber, the reactants enter the "vortex chamber," which is oriented perpendicularly to the plane of the channels. In the four-jet tangential ABAB stainless-steel mixer and all of the Plexiglass mixers, the vortex chamber and mixing chamber are located in the *Pt* inlay (Fig. 1 and Table 1). The *Pt* inlay (20 μm orifice, 3 mm in outer diameter, and 100 μm thick; obtained from Baltic Preparation) also acts as a seal and is mounted on top of the channels and the premixing chamber and is fixed with a fine threaded screw cap (not shown in Fig. 1, but see in Ref. [25]) to the mixer body. The shape of the *Pt* vortex chamber is conical, whereas the shape of the mixing chamber is cylindrical (Fig. 1 and Table 1). The volume of the mixing chamber is only 10 pl (Table 1). In the glass–silicon mixer, the vortex chamber is cylindrical and very long (257 μm) owing to the thickness of the silicon (Table 1 and Fig. 2). The vortex chamber of the glass–silicon mixer ends in a cylindrical mixing chamber (silicon orifice) with diameters between 25 and 70 μm (see Supplementary Fig. 1 in online Supplementary material). In all mixers, the mixed fluids leave the orifice as a free jet. More details are provided in the Supplementary material.

Results and discussion

To determine the mixing efficiency of the turbulent micro-mixers, the appearance or quenching of fluorescence of 8-hydroxypyrene-1,3,6-trisulfonic acid (HPTS) in acid–base reactions was determined in a free jet (Fig. 3 and Section 5A of Supplementary material). In these experiments, a low (1.5-fold) excess of acid over base (or vice versa) was used to ensure that fluorescence quenching (or disappearance) is due to near stoichiometric encounter of H_3O^+ and OH^-, a prerequisite to assess mixing efficiency. As a result of this experimental condition, fluorescence quenching (or disappearance) or mixing efficiency can be calculated only when the reaction has progressed for more than two-thirds (Fig. 3 and Section 5A of Supplementary material). The four-jet tangential ABAB stainless-steel mixer mixes the reactants for more than 90% at $Re \sim 500$, and full mixing is obtained at $Re > 1000$ to 1500. The Plexiglass analogue of this mixer and the two-jet tangential Plexiglass mixer behave similarly, given the experimental error (Fig. 3), although full mixing by the latter mixers might require somewhat higher $Re \sim 2000$ to 2500. The four-jet AABB Plexiglass

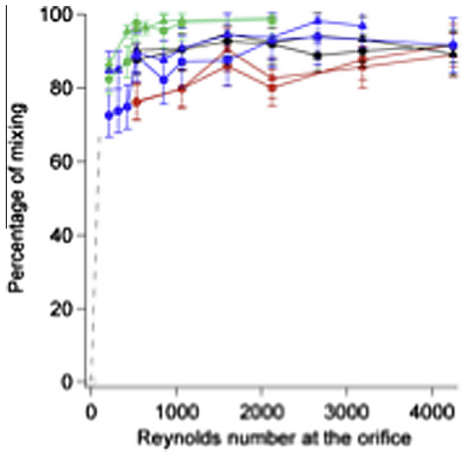

Fig.3. Percentage of mixing by tangential micro-mixers observed in a free-flowing jet (20 μm diameter). Shown are the four-jet tangential ABAB stainless-steel mixer (green ● and ▲) with fluorescence standard error values of ± 4.9 and 1.8%, respectively, the four-jet tangential ABAB Plexiglass mixer (blue ● [± 8.0%] and ▲ [± 6.1%]), the four-jet AABB Plexiglass mixer (red ● [± 6.2%] and ▲ [± 6.6%]), and the two-jet AB Plexiglass mixer (black ● [± 4.8%] and ▲ [± 6.6%]). Fluorescence appearance/quenching was monitored using HPTS in deprotonation (●)/protonation (▲) reactions, respectively. NaOH/HCl ratio was 15/10 mM = 1.5 for deprotonation and the reverse for protonation. [HPTS] = 1.5 mM. The dotted line (from zero to 66.7% fluorescence) indicates the threshold below which the percentage mixing cannot be calculated (see Section 5A of Supplementary material). (For interpretation of the references to color in this figure legend, the reader is referred to the Web version of this article.)

mixer is less efficient, showing a maximal amount of mixing obtained at $Re > 3000$. Therefore, we conclude that the two-jet and four-jet ABAB tangential micro-mixers with alternating reactant channels have similar mixing qualifications and that the AABB configuration performs less efficiently, presumably due to a smaller contact area between the fluid flows. The AABB mixer configuration is often used in rapid freeze-quench instruments [1,2,46] and, thus, can easily be improved. Unfortunately, the experiment shown in Fig. 3 could not be successfully performed with the four-jet tangential ABAB glass–silicon mixers due to difficulties of forming a stable free jet, preventing direct quantitative assessment of the mixing efficiency. However, we could confirm by eye that the jet emanating from the glass–silicon mixers is fluorescent and, hence, that the fluids are mixed for more than 66.7% (cf. the ordinate in Fig. 3).

To determine the actual mixing time of the micro-mixers, one should determine whether the mixing occurs exclusively in the relatively small mixing compartment or already to some extent earlier in the larger vortex chamber and/or premixing chamber. Mixing, or rather premixing, in the vortex or premixing chamber would constitute a dead volume that would add to the total dead time, for example, in a setup where the micro-mixers are integrated with an optical cell to monitor the kinetics of (bio)chemical

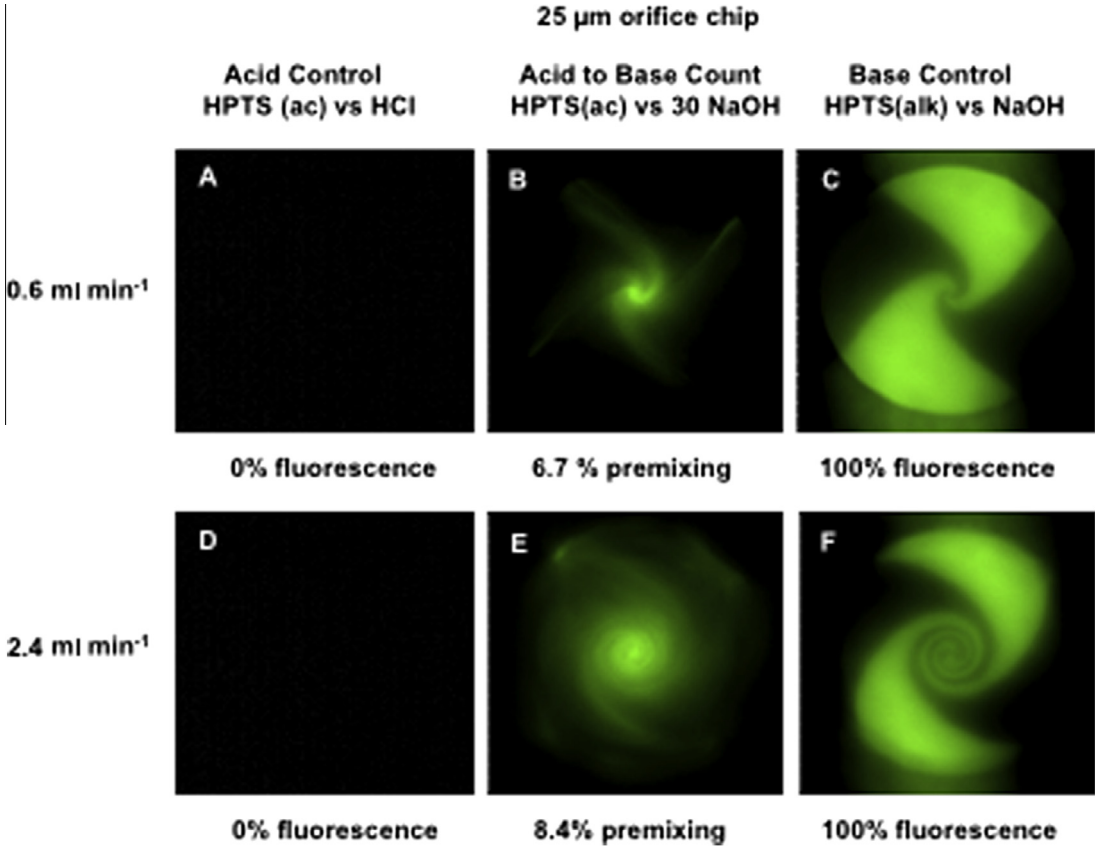

Fig.4. Determination of the amount of premixing in the vortex chamber. Fluorescence appearance due to deprotonation of HPTS was measured in the vortex chamber of the glass–silicon chip (25 µm orifice diameter) at flow rates of 0.6 ml min^{-1} (A–C) and 2.4 ml min^{-1} (D–F). (A, D) HPTS in HCl versus HCl (zero fluorescence control). (B, E) HPTS in HCl versus 30-fold excess NaOH. (C, F) HPTS in NaOH versus NaOH (100% fluorescence control). See Section 5 of Supplementary material for initial and final [HCl], [NaOH], and [HPTS]. Images are 125 × 125 µm, the diameter of the vortex chamber is 100 µm, and the microscope focus is halfway into the vortex chamber (see Supplementary Fig. 3).

reactions. To determine where and to what extent premixing occurs, fluorescence measurements were performed in the optically transparent vortex chamber of the four-jet tangential ABAB glass–silicon mixers (Figs. 4 and 5). In these experiments, a high (30-fold) excess of base over acid was used to determine the maximal rate of diffusion of OH^- across the fluid boundaries and, thus, the maximal extent of premixing in the vortex chamber. The images of the vortex chamber (diameter of 100 µm and 257 µm in length; see Table 1 and Fig. 2) were recorded with the inverted microscope focused approximately halfway into the vortex chamber (see Supplementary Fig. 3). In the very center (Fig. 4) or slightly off-center (Fig. 5), the intense fluorescence is due mainly to the mixing in the mixing chamber where the jet leaves the mixer. To determine the degree of premixing, this central fluorescence was subtracted from the total fluorescence (see Section 5 of Supplementary material). The fluid flow profiles recorded for the controls (Fig. 4C and F) at low and high fluid flow rates show near irrotational and rotational flow patterns, respectively, in good agreement with calculations in Ref. [27]. There is very little cross-boundary diffusion of the fluorescent dye. This is further confirmed in the other images of Fig. 4, which indicate only 6.7 to 8.4% premixing due to diffusion across the boundary. Although the mixer with a 70-µm orifice (Fig. 5) would require higher flow rates to produce full mixing in the mixing chamber (*Re* > 2000), the observed amount of premixing remains quite low (11.5–16.9%).

Fig. 6 and Supplementary Table 1 (see Supplementary material) summarize the premixing behavior of the four glass–silicon mixers with different dimensions of the mixing chamber (orifices of 25, 30, 50, and 70 µm); however, note that all mixers have the same dimensions of the vortex chamber. Fig. 6 shows that at a given flow rate, the amount of premixing is fairly independent of the orifice diameter. The calculated *Re* values increase in the premixing chamber from 13 to 265, and in the vortex chamber from 27 to 531, with increasing flow rates from 0.5 to 10 ml min^{-1}. The increased *Re* in premixing and vortex chambers could explain why the amount of premixing increases with fluid flow rate (but apparently not for the mixer with a 50-µm orifice for reasons currently unknown; see Fig. 6) even though the flow is predominantly laminar. The laminar flow regime is suggested by the approximately linear relation between fluid flow rate (and thus *Re*) in the vortex chamber and the percentage premixing (Fig. 6). Because the geometries of the glass–silicon mixer and the stainless-steel mixer are very similar, they are expected to produce very similar mixing and premixing profiles. Thus, the onset of mixing in the glass–silicon mixers occurs at similar *Re* values (~500–1000; see Fig. 3) and appears complete at *Re* ~ 1500 to 2000. Fig. 6 indicates that at these latter *Re* values needed for complete mixing, the premixing amount varies from approximately 9% (for a 25-µm orifice) to 15% (for a 70-µm orifice). The low amount of premixing is a key requirement to minimize mixing dead times.

Although the amount of premixing could not be directly determined in the stainless-steel mixer (20-µm orifice), it is possibly even lower than the approximately 9% observed for the glass–silicon mixer with the 25-µm mixing chamber (orifice) because the length of the vortex chamber is shorter (67 vs. 257 µm; see Fig. 1). This implies a shorter time for diffusion of reagents across the tangential fluid boundaries and, hence, a lower degree of premixing. For the stainless-steel mixer, the shortest calculated residence time of the liquids in the vortex chamber

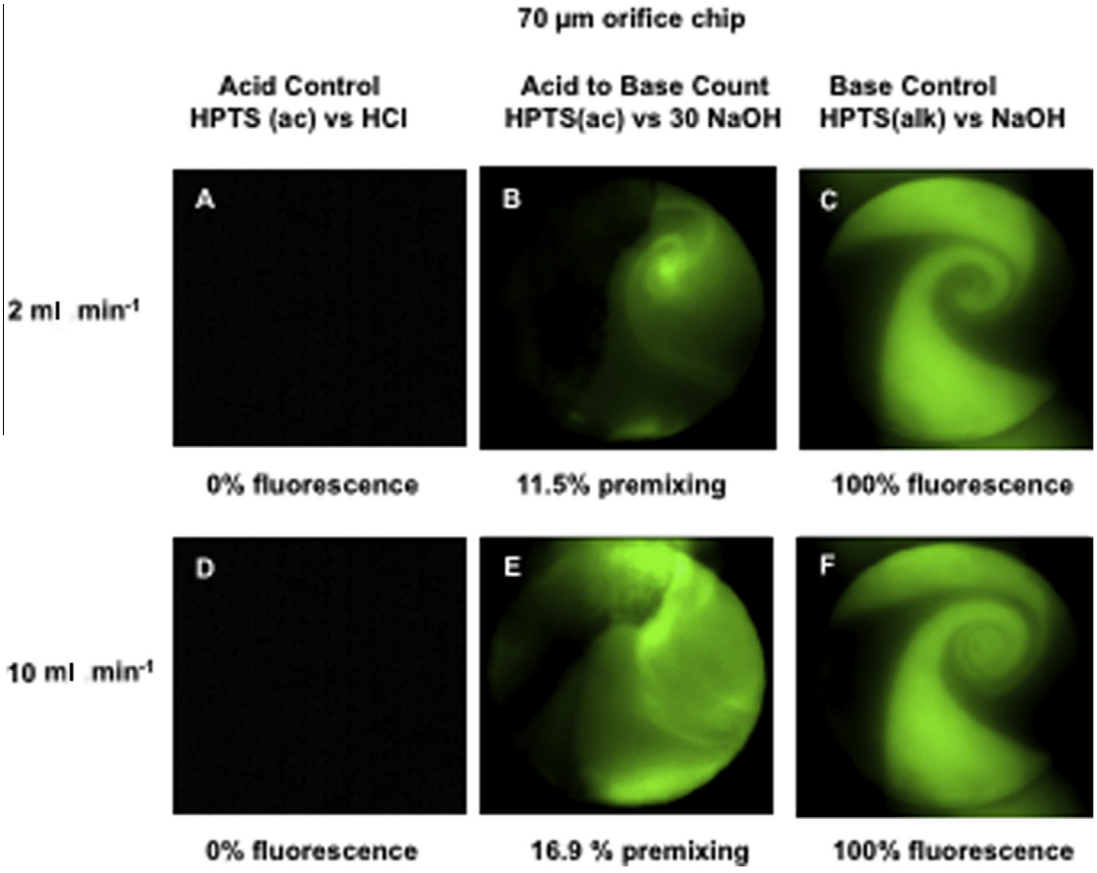

Fig.5. Determination of the amount of premixing in the vortex chamber. Fluorescence appearance due to deprotonation of HPTS was measured in the vortex chamber of the glass–silicon chip (70 µm orifice diameter) at flow rates of 2.0 ml min^{-1} (A–C) and 10.0 ml min^{-1} (D–F). (A, C) HPTS in HCl versus HCl (zero fluorescence control). (B, E) HPTS in HCl versus 30-fold excess NaOH. (C, F) HPTS in NaOH versus NaOH (100% fluorescence control). See Section 5 of Supplementary material for initial and final [HCl], [NaOH], and [HPTS]. Images are 125 × 125 µm, the diameter of the vortex chamber is 100 µm, and the microscope focus is halfway into the vortex chamber (see Supplementary Fig. 3).

(V = 90 pl, $Re \sim 417$) is 1.4 µs at the maximal flow rate of 4 ml min^{-1}; under these same flow conditions, there is 9% or less premixing in the glass–silicon mixer (Fig. 6), which we assume to be true for the stainless-steel mixer in view of their similar geometries. At the flow rate of 4 ml min^{-1}, the reactants are completely mixed (Fig. 3), whereas the residence time in the mixing chamber of the stainless-steel mixer (V = 10 pl, $Re \sim 4246$) is only 160 ns. This also means that complete mixing is achieved within 160 ns. Even at flow rates of 2 ml min^{-1} ($Re \sim 2100$, where the fluids are completely mixed; see Fig. 3), a maximal mixing time of just approximately 310 ns is calculated with the advantage that the ambient pressure is greatly reduced (~4-fold to ~10 MPa). Because the great majority of the glass–silicon micro-mixers were stable at pressures of 10 MPa, they can indeed be employed for large-scale production of nanosecond mixers. We further point out that the extent of premixing determined here using a pH-sensitive dye is considered an upper limit given that H^+ and OH^- diffusion constants are approximately 10 times and 5 times larger, respectively, than those of other small ions. In conclusion, the turbulent micro-mixers do completely mix liquids within 160 ns with little premixing.

Pressure buildup is a necessary consequence of the high linear fluid velocities in turbulent (micro-) mixers. The high flow rates and pressures reported here are provided by HPLC pumps that operate up to 40 MPa. The great majority of proteins are stable at these pressures [47], further indicated by the general experience that these HPLC pumps can be used for purification of native active proteins and enzymes by column chromatography. In our freeze-quench experiments using the same HPLC setup and stainless-steel mixer described here, we have never encountered denaturation problems and the rate constants determined at 20 to 40 MPa by us [28,43,44,48,49] are similar to those determined by others working at ambient pressures [5,6,8,12]. In general, oligomeric proteins start to dissociate at pressures of 100 to 200 MPa, and monomeric proteins denature at approximately four times higher pressures [47]. In view of the quadratic relation between pressure and fluid flow rate (Eq. (2)), the micro-mixers described here could be used at approximately 2-fold higher flow rates before protein denaturation sets in, potentially decreasing the mixing time to less than 100 ns.

By measuring both the premixing characteristics and mixing performance, we reason that the key design aspects for a micro-mixer that mixes liquids in nanoseconds are the ABAB configuration of the four-jet tangential mixer in which the channels are offset by one-half to one channel diameter. This offset creates a vortex of four fluids that rotate around one another, which leads to a decrease in the diffusion distances and improves the mixing performance. As a result, (near) complete mixing occurs at $Re \sim 1000$ to 1500 (Fig. 3), which is well below the value of 2040 ± 10 for the onset of sustained turbulent flow in a pipe [24]. Although a two-jet tangential mixer might be as efficient as a four-jet tangential mixer (Fig. 3), the extension to 8 or 16 tangential fluid channels leads to more or even complete premixing in the vortex chamber [29]. This behavior is certainly suitable for lab-on-a-chip applications where a 1-ms time resolution is adequate, but not for the design of instruments with (sub)microsecond time resolution. For such devices, premixing

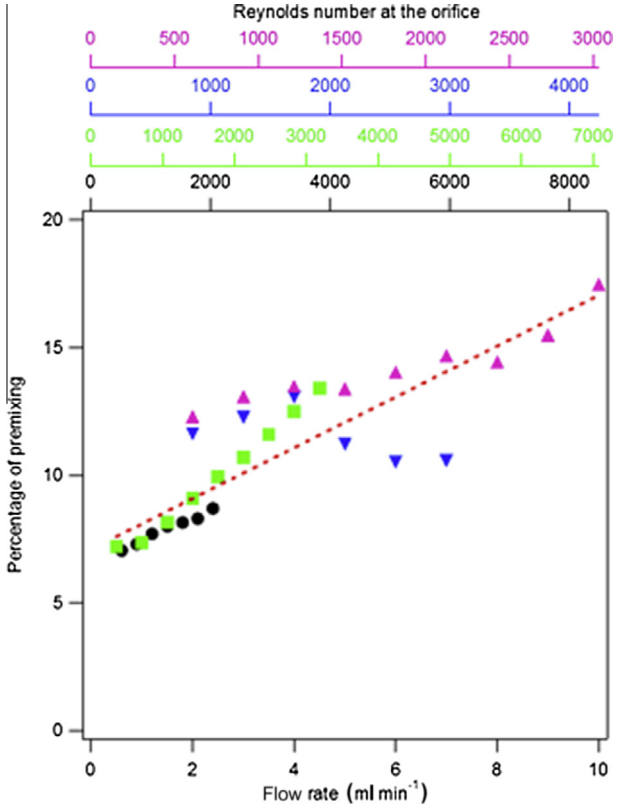

Fig.6. Percentage of premixing in the vortex chamber of the glass–silicon micro-mixer chips with orifice diameters of 25 μm (black ●), 30 μm (green ◙), 50 μm (blue ▼), and 70 μm (purple ▲). Experimental data of the fluorescence appearance during deprotonation of HPTS (HPTS in HCl vs. 30-fold excess NaOH) are shown as averaged values of three independent measurements (two for 70 μm) as a function of both flow rate and Reynolds number in the mixing chamber at the orifice, Re_{mix}. Full mixing in the orifice is at *Re* 1000 to 1500. The dotted straight line is a linear fit to all data points with a slope of 0.0137 (% premixing/*Re*). Individual slopes are 0.0215 (25 μm), 0.029 (30 μm), −0.006 (50 μm), and 0.0096 (70 μm). Standard deviation for triplicates (duplicates) equals ± 0.04 times the measured values. (For interpretation of the references to color in this figure legend, the reader is referred to the Web version of this article.)

should be prevented as much as possible. To minimize the amount of premixing, the height (or length) of the vortex chamber should be as small as possible to reduce the retention time for diffusion across the fluid boundaries. On the other hand, the diameter of the vortex chamber should be as large as possible with respect to the diameter of the mixing chamber. This will maximize the ratio of the *Re* values in the mixing chamber and vortex chamber and, thus, minimize premixing resulting from turbulence at the fluid boundaries. The ratio of the diameters of the mixing chamber and vortex chamber in the designs used here, three for the stainless-steel and Plexiglass mixers and four for the glass–silicon mixer, yield less than 9% premixing in the vortex chamber under conditions that complete mixing occurred in the mixing chamber in nanoseconds. The future challenge is to integrate an optical cell with the micro-mixer that would allow spectroscopic observations in nanoseconds, thereby enabling study of the very onset of chemical reactions in general and of enzyme catalysis in particular.

Acknowledgments

This work was supported by NanoNed (project TAC.6380). The authors greatly acknowledge the contributions made to the designs of the Plexiglass mixers by M. Langeveld. We also are thankful to P. D. E. M. Verhaert (Delft University of Technology) for making available to us the Nikon Eclipse inverted microscope.

Appendix A. Supplementary data

Supplementary data associated with this article can be found, in the online version, at http://dx.doi.org/10.1016/j.ab.2014.10.003.

References

[1] S. de Vries, Freeze-quench kinetics, in: R.A. Scott, C.M. Lukehart (Eds.), Encyclopedia of Inorganic Chemistry, John Wiley, New York, 2007, pp. 125–142.
[2] S. Mitic, S. de Vries, Rapid mixing techniques for the study of enzyme catalysis, in: E.H. Egelman (Ed.), Comprehensive Biophysics, Academic Press, Oxford, UK, 2012, pp. 514–532.
[3] A.H. Zewail, Femtochemistry: atomic-scale dynamics of the chemical bond using ultrafast lasers [Nobel Lecture], Angew. Chem. Int. Ed. Engl. 39 (2000) 2586–2631.
[4] R.E. Blankenship, Molecular Mechanisms of Photosynthesis, Blackwell, Oxford, UK, 2002.
[5] P. Brissette, D.P. Ballou, V. Massey, Determination of the dead time of a stopped-flow fluorometer, Anal. Biochem. 181 (1989) 234–238.
[6] V.B. Borisov, E. Forte, P. Sarti, A. Giuffre, Catalytic intermediates of cytochrome *bd* terminal oxidase at steady-state: ferryl and oxy-ferrous species dominate, Biochim. Biophys. Acta 2011 (1807) 503–509.
[7] M.C. Shastry, S.D. Luck, H. Röder, A continuous-flow capillary mixing method to monitor reactions on the microsecond time scale, Biophys. J. 74 (1998) 2714–2721.
[8] H. Röder, K. Maki, H. Cheng, Early events in protein folding explored by rapid mixing methods, Chem. Rev. 106 (2006) 1836–1861.
[9] S. Matsumoto, A. Yane, S. Nakashima, M. Hashida, M. Fujita, Y. Goto, S. Takahashi, A rapid flow mixer with 11-μs mixing time microfabricated by a pulsed-laser ablation technique: observation of a barrier-limited collapse in cytochrome *c* folding, J. Am. Chem. Soc. 129 (2007) 3840–3841.
[10] K.A. Dill, J.L. MacCallum, The protein-folding problem, 50 years on, Science 338 (2012) 1042–1046.
[11] J. Kubelka, T.K. Chiu, D.R. Davies, W.A. Eaton, J. Hofrichter, Sub-microsecond protein folding, J. Mol. Biol. 359 (2006) 546–553.
[12] O. Einarsdottir, C. Funatogawa, T. Soulimane, I. Szundi, Kinetic studies of the reactions of O_2 and NO with reduced *Thermus thermophilus* ba_3 and bovine aa_3 using photolabile carriers, Biochim. Biophys. Acta 2012 (1817) 672–679.
[13] S.J. Chen, RNA folding: conformational statistics, folding kinetics, and ion electrostatics, Annu. Rev. Biophys. 37 (2008) 197–214.
[14] A. Fersht, Structure and Mechanism in Protein Science, W. H. Freeman, New York, 1999.
[15] J.N. Abelson, M.I. Simon, G. Marriott (Eds.), Methods in Enzymology, Vol. 291: Caged compounds, Academic Press, San Diego, 1998.
[16] H.B. Gray, J.R. Winkler, Photoinduced electron transfer in ruthenium-modified cytochrome *c*, Pure Appl. Chem. 64 (1992) 1257–1262.
[17] H. Hartridge, F.J.W. Roughton, A method of measuring the velocity of very rapid chemical reactions, Proc. R. Soc. London A 104 (1923) 376–394.
[18] H. Hartridge, F.J.W. Roughton, Improvements in the apparatus for measuring the velocity of very rapid chemical reactions (part II), Proc. Cambr. Phil. Soc. 23 (1927) 450–460.
[19] B. Chance, The accelerated flow method for rapid reactions, J. Franklin Inst. 229 (1940) 737–766.
[20] P. Regenfuss, R.M. Clegg, M.J. Fulwyler, F.J. Barrantes, T.M. Jovin, Mixing liquids in microseconds, Rev. Sci. Instrum. 56 (1985) 283–290.
[21] Z.K. Majumdar, J.D.B. Sutin, R.M. Clegg, Microfabricated continuous-flow, turbulent, microsecond mixer, Rev. Sci. Instrum. 76 (2005) 1–11.
[22] S.Y. Jin, Y.Z. Liu, W.Z. Wang, Z.M. Cao, H.S. Koyama, Numerical evaluation of two-fluid mixing in a swirl micro-mixer, J. Hydrodynam. B 18 (2006) 542–546.
[23] T.T. Veenstra, T.S.J. Lammerink, M.C. Elwenspoek, A. van den Berg, Characterization method for a new diffusion mixer applicable in micro flow injection analysis systems, J. Micromech. Microeng. 9 (1999) 199–202.
[24] C.H. Lin, C.H. Tsai, L.M. Fu, A rapid three-dimensional vortex micromixer utilizing self-rotation effects under low Reynolds number conditions, J. Micromech. Microeng. 15 (2005) 935–943.
[25] K.E. Herold, A. Rasooly (Eds.), Lab on a Chip Technology, Vol. 1: Fabrication and Microfluidics, Caister Academic Press, Norfolk, UK, 2009.
[26] A. van den Berg, T.S.J. Lammerink, Microsystem technology, in: A. Mans, H. Becker (Eds.), Chemistry and Life Science, Vol. 194, Springer, Berlin, 1998, pp. 21–49.
[27] K. Avila, D. Moxey, A. de Lozar, M. Avila, D. Barkley, B. Hof, The onset of turbulence in pipe flow, Science 333 (2011) 192–196.
[28] A.V. Cherepanov, S. de Vries, Microsecond freeze-hyperquenching: development of a new ultrafast micro-mixing and sampling technology and application to enzyme catalysis, Biochim. Biophys. Acta 1656 (2004) 1–31.
[29] A.A.S. Bhagat, E.T.K. Peterson, I. Papautsky, A passive planar micromixer with obstructions for mixing at low Reynolds numbers, J. Micromech. Microeng. 17 (2007) 1017–1024.
[30] J.J. Chen, C.H. Chen, Investigation of swirling flows in mixing chambers, Model. Simul. Eng. 2011 (2011) 1–15.
[31] R.H. Liu, M.A. Stremler, K.V. Sharp, M.G. Olsen, J.G. Santiago, R.J. Adrian, H. Aref, D.J. Beebe, Passive mixing in a three-dimensional serpentine microchannel, J. Microelectromech. Syst. 9 (2000) 190–197.

[32] S. Bohm, K. Greiner, S. de Vries, A. van den Berg, A rapid vortex micromixer for studying high-speed chemical reactions, in: J.M. Ramsey, A. van den Berg (Eds.), Micro Total Analysis System, Kluwer, Dordrecht, Netherlands, 2001, pp. 25–27.
[33] M. Kakuta, P. Hinsmann, A. Manz, B. Lendl, Time-resolved Fourier transform infrared spectrometry using a microfabricated continuous flow mixer: application to protein conformation study using the example of ubiquitin, Lab Chip 3 (2003) 82–85.
[34] W. Ehrfeld, K. Golbig, V. Hessel, H. Lowe, T. Richter, Characterization of mixing in micromixers by a test reaction: single mixing units and mixer arrays, Ind. Eng. Chem. Res. 38 (1999) 1075–1082.
[35] R. Masuch, D.A. Moss, Stopped flow apparatus for time-resolved Fourier transform infrared difference spectroscopy of biological macromolecules in $1H_2O$, Appl. Spectrosc. 57 (2003) 1407–1418.
[36] D.E. Hertzog, B. Ivorra, B. Mohammadi, O. Bakajin, J.G. Santiago, Optimization of a microfluidic mixer for studying protein folding kinetics, Anal. Chem. 78 (2006) 4299–4306.
[37] D.E. Hertzog, X. Michalet, M. Jäger, X. Kong, J.G. Santiago, S. Weiss, O. Bakajin, Femtomole mixer for microsecond kinetic studies of protein folding, Anal. Chem. 76 (2004) 7169–7178.
[38] J.B. Knight, A. Vishwanath, J.P. Brody, R.H. Austin, Hydrodynamic focusing on a silicon chip: mixing nanoliters in microseconds, Phys. Rev. Lett. 80 (1998) 3863–3866.
[39] S. Yao, O. Bakajin, Improvements in mixing time and mixing uniformity in devices designed for studies of protein folding kinetics, Anal. Chem. 79 (2007) 5753–5759.
[40] S.A. Pabit, S.J. Hagen, Laminar-flow fluid mixer for fast fluorescence kinetics studies, Biophys. J. 83 (2002) 2872–2878.
[41] Y. Gambin, C. Simonnet, V. VanDelinder, A. Deniz, A. Groisman, Ultrafast microfluidic mixer with three-dimensional flow focusing for studies of biochemical kinetics, Lab Chip 10 (2010) 598–609.
[42] S.A. Waldauer, L. Wu, S. Yao, O. Bakajin, L.J. Lapidus, Microfluidic mixers for studying protein folding, J. Vis. Exp. 62 (2012) e3976, http://dx.doi.org/10.3791/3976.
[43] F.G.M. Wiertz, Electron transfer and proton pumping pathways in cytochrome aa_3 (PhD thesis), Delft University of Technology, 2007.
[44] F.G. Wiertz, O.M. Richter, B. Ludwig, S. de Vries, Kinetic resolution of a tryptophan-radical intermediate in the reaction cycle of *Paracoccus denitrificans* cytochrome *c* oxidase, J. Biol. Chem. 282 (2007) 31580–31591.
[45] E.T. Carlen, J.G. Bomer, J.W. van Nieuwkasteele, A. van den Berg, Silicon and glass micromachining, in: K.E. Herold, A. Rasooly (Eds.), Lab on a Chip Technology, Vol. 1: Fabrication and Microfluidics, Caister Academic Press, Norfolk, UK, 2009, pp. 83–114.
[46] D.P. Ballou, G.A. Palmer, Practical rapid quenching instrument for the study of reaction mechanisms by electron paramagnetic resonance spectroscopy, Anal. Chem. 46 (1974) 1248–1253.
[47] V.V. Mozhaev, K. Heremans, J. Frank, P. Masson, C. Balny, High pressure effects on protein structure and function, Proteins 24 (1996) 81–91.
[48] K.A. Sam, M.J.F. Strampraad, S. de Vries, S.J. Ferguson, Very early reaction intermediates detected by microsecond time scale kinetics of cytochrome cd_1-catalyzed reduction of nitrite, J. Biol. Chem. 283 (2008) 27403–27409.
[49] A. Paulus, S.H.G. Rossius, M. Dijk, S. de Vries, An oxoferryl–porphyrin radical catalytic intermediate in cytochrome *bd* oxidases protects cells from the formation of reactive oxygen species, J. Biol. Chem. 287 (2012) 8830–8838.